Article

Applied Spectroscopy

Applied Spectroscopy
0(0) 1–10

DOI: 10.1177/0003702816651891
asp.sagepub.com
SAGE

Structural Characterization of the Intrinsically Disordered Protein p53 Using Raman Spectroscopy

Sara Signorelli[1,2], Salvatore Cannistraro[1], and Anna Rita Bizzarri[1]

Abstract

The intrinsically disordered protein p53 has attracted a strong interest for its important role in genome safeguarding and potential therapeutic applications. However, its disordered character makes difficult a full characterization of p53 structural architecture. A deep knowledge of p53 structural motifs could significantly help the understanding of its functional properties, in connection with its complex binding network. We have applied Raman spectroscopy to investigate the structural composition and the conformational heterogeneity of both full-length p53 and its DNA binding domain (DBD), in different solvent environments. In particular, a careful analysis of the Amide I Raman band, which is highly sensitive to protein secondary structure elements such as α-helices, β-sheets and random coils, has revealed the presence of extended random coils in p53 and predominant β-sheet regions in its DBD. In addition, this analysis has allowed us to explore the ensemble of interchanging conformations in both p53 and its DBD, highlighting a higher conformational heterogeneity in p53 than in its DBD. Furthermore, by applying a principal components analysis, we have identified the principal spectral markers in both p53 and DBD samples. The combination of the two approaches could be insightful for the study of intrinsically disordered proteins, by offering increased versatility and wide application as a label-free, real-time and non-invasive detection method.

Keywords

Raman spectroscopy, p53, intrinsically disordered protein, heterogeneity, amide I band, deconvolution, principal component analysis

Date received: 24 December 2015; accepted: 2 May 2016

Introduction

Intrinsically disordered proteins (IDPs) are a newly recognized class of proteins that, under physiological conditions, lacking a unique, well-defined 3D structure, carry out functions by means of unstructured regions whose amino acid composition prevents autonomous folding.[1] Indeed, these proteins, when unbound, populate an ensemble of diverse, interconverting and thermodynamic stable conformations, which are suitable for various functional purposes.[2] This property provides IDPs with a larger interaction surface area than globular proteins and confers inherent flexibility and intrinsic plasticity allowing a single protein to recognize a large number of biological targets without sacrificing specificity.[3,4] Remarkably, the conformational disorder is significantly enriched in proteins associated with transcription, signaling, cell cycle and other regulated biological processes,[5,6] underlying a strict correlation of altered expressions of IDPs with several disease conditions such as cancer and neurodegeneration.[7–11]

Within this context, we have focused our attention on the p53 IDP that is a master protein in tumor regulation, with a crucial onco-suppression role.[12] The p53 protein works as a homotetramer, in which each monomer is composed by three principal domains. A large transactivation domain (N-terminal, residues 1–70) and a regulatory domain (C-terminal, residues 324–355) have been shown to be intrinsically unfolded with a weak tendency in solution

[1]Biophysics and Nanoscience Centre, Università della Tuscia, Italy
[2]Department of Science, University Roma Tre, Italy

Corresponding author:
Anna Rita Bizzarri, Largo dell Università Viterbo 01100 Italy.
Email: bizzarri@unitus.it

to form a compact secondary structure, upon binding to their partners.[13–15] A DNA core domain (DBD, residues 94–293) has been found to have a relatively stable structure composed by an immunoglobulin-like central β-sandwich of two antiparallel β-sheets, which provides the basic scaffold for the DNA-binding surface.[16,17]

The presence of the large unstructured regions allows p53 to act as a central hub for a plethora of signaling pathways that control cell proliferation and death in response to potentially oncogenic conditions.[18] A wide array of covalent modifications and protein interactions modulate the nuclear and cytoplasmic activities of p53.[19–25] Notably, p53 is characterized by missense or deletion mutations, chiefly in the core DNA-binding domain,[26–28] in approximately 75% of human cancers, with drastic effects on its functionality.[29] Accordingly, the knowledge of the structural properties of p53 is a key point for both understanding its functional role and developing effective anticancer strategies.[30]

Although a number of biophysical techniques have been applied to study the structure of p53, a complete characterization of its structural conformation is far from being reached.[31–34]

Raman spectroscopy has several important advantages in revealing secondary structural information of the intrinsically disordered proteins and peptides.[35,36] Indeed, Raman spectra of a protein in solution is constituted by the collection of signals arising from each conformation present in the ensemble, thus providing an "instantaneous snapshot" of the protein populations.[36]

On such a basis, we have applied Raman spectroscopy to characterize the secondary structure and even the population heterogeneity of the full-length p53 and its DBD region. In particular, the Amide I Raman band, which contains information on the secondary structure of the protein molecules, has been investigated in different solvent environments by applying two different approaches. First, we have carried out a fitting procedure for the Amide I band, already validated on several proteins and recently applied on intrinsically disordered proteins and peptides.[36,37] In particular, the band has been deconvolved in terms of three components separately associated with the α-helix, β-sheet and random coil structures.[36] In this way, remarkable information on both the secondary structure motifs of the two proteins and their conformational disorder could be obtained. Additionally, Amide I bands have been analyzed through the principal components analysis (PCA) technique. Principal components analysis is a multivariate analysis method that allows one to reduce a multi-dimensional dataset by retaining the characteristics of the original ensemble mostly contributing to its variance. Briefly, a limited number of variables, known as principal components (PCs), contain most of the spectral information and they can be divided into scores and loadings. The former ones represent the distribution of the spectra for a given PC and reveal the relations existing among the samples. The latter ones represent how much a variable, or range of variables, influences a given PC. Indeed, PCA is particularly effective for categorizing Raman spectra that are otherwise hardly distinguishable.[38–41] Herein, we have used this technique to single out the main spectral band of p53 and DBD leading to a clear discrimination between the p53 protein and its DBD according to their secondary structures and even among their structural modulation as induced by solvent changes.

The involvement of IDPs in a broad range of physiological functions as well as their impairment connected with a wide variety of disease states deserve a large interest for their detailed structural elucidation. In this regard, our findings could deepen knowledge of the p53 protein and its DBD region, in light of a possible contribution to the development of drugs for innovative anticancer strategies.

Materials and Methods

Chemicals and Sample Preparation

High quality wild-type, full-length p53 (human) recombinant protein (purity >95%) was purchased from Thermo Scientific. DNA binding domain (a.a 81-300) was kindly provided by the Translational Oncogenomic Unit of the Italian National Cancer Institute 'Regina Elena'-IFO. All samples were dissolved in three solvents: (i) phosphate buffer solution (PBS, 95.3% H_2O, 3.8% NaCl, 0.1% di KCl, 0.7% Na_2HPO_4, 0.1% KH_2PO_4; pH = 7.5); (ii) 50% methanol (MeOH, CH_3OH; Carlo Erba) and 50% PBS; (iii) 50% 2,2,2 Trifluoroethanol (TFE, CF_3CH_2OH; Sigma-Aldrich, St. Louis, MO), and 50% PBS. The concentration of each sample was 60 μM. We will refer below to wild-type full-length p53 and its DNA binding domain as p53 and DBD, respectively.

Raman Spectroscopy

A Jobin-Yvon Super Labram confocal system was used to acquire Raman spectra. It was equipped with a liquid nitrogen-cooled charge coupled device (CCD) (EEV CCD10-11 back illuminated; pixel format: 1024 × 128 detector and a spectrograph with a 1800 g/mm grating allowing a resolution of 5 cm^{-1}. Back-scattering geometry for spectra collection was applied and a notch filter to reject the elastic contribution was used. A diode-pumped solid-state laser emitting at 532 nm with a power of 10 mW (4.4 mW on the sample) was employed as the excitation source. Measurements were collected using a 50× objective with a numerical aperture (NA) = 0.6 (laser spot diameter reaching the sample was about 1 μm). A confocal diaphragm of 400 μm and a slit of 200 μm were chosen as optimal acquisition parameters. Raman experiments were performed on specimen drops deposited on optical glass, at room temperature.

Thirty Raman spectra for each sample were collected from different points of the drops, each one with an acquisition time of 180 s. In order to check the protein hydration level, we monitored the ratio between the water band (3000–3700 cm^{-1}) and the Amide I band (1625–1700 cm^{-1}); such a ratio did not vary by more than 5% during the acquisition time in all the spectra. Furthermore, no variation in the Amide I band spectral features (i.e., changes in shape or in vibrational frequency) was observed during the acquisition time. All Raman spectra were vector normalized within the whole wavenumber range and processed by a baseline correction. In most instances a linear baseline correction was applied. The few spectra showing a fluorescence background were corrected with the rubber band method consisting of the stretching of a line between spectrum endpoints, as it follows the spectrum minima.

Curve-fitting Procedure

Band fitting of the Raman Amide I band and assignments to the structural components were performed according to Maiti et al.,[36] whose approach was validated on other IDPs.[35] Accordingly, Amide I regions were dissected in term of three curves associated to α-helical conformations (at about 1655 cm^{-1}), β-sheet structures (1667 cm^{-1}) and random coil regions (at about 1680–1685 cm^{-1}). The spectral peaks at 1550 cm^{-1}, 1580 cm^{-1}, 1604 cm^{-1} and 1615 cm^{-1} needed to be included to account for modes of tryptophan (Trp),[42] Phenylalanine (Phe),[43] Phe and tyrosine (Tyr)[36] residues, respectively, since they were not baseline separated from Amide I features. Moreover, accurate fitting of the experimental profile required an additional feature near 1637 cm^{-1} (1630–1645 cm^{-1}), probably due to disordered structure and/or vibronic coupling.[43] Since we are interested in the secondary structure contributions, the structural percentages were calculated by determining the areas of the fitting bandwidth at half height (BWHH) corresponding to the α-helical, β-sheet and random coil components. The curve-fitting procedure was performed using the OPUS software version 6.5, which applies the Levenberg–Marquardt minimization algorithm (LMA) and pseudo-Voigt functions as peak profiles. The area errors were evaluated by repeating the curve-fitting procedure on ten different spectra, with the goodness of the fits being assessed by the reduced chi-square value.

Principal Component Analysis

In this study, PCA was applied to three data sets: (i) full-length p53 and DBD Raman spectra in PBS (number of spectra $n = 55$), being satisfactorily described by a number of components $N = 53$; (ii) DBD Raman spectra in the three solvents ($n = 67$; $N = 80$) and (iii) full-length p53 Raman spectra in the three solvents ($n = 73$; $N = 77$). The correlation matrix was analyzed and the number of components to be considered was defined as the number of components required to explain at least the 80% of total variance. STATISTICA 7.0 software (StatSoft Inc. USA, 2004) was used for all the analyses.

Results and Discussion

Analysis of the Protein Structural Motifs and Heterogeneity

The Raman spectra of DBD in PBS is shown in Figure 1 (upper spectrum). The spectrum presents a complex set of peaks and overlapping bands among which the main Raman features due to aromatic amino acids and polypeptide chain can be recognized.[35] The same general features are shown for p53 in PBS (Figure 1 lower spectrum) even if small shifts in frequency and some variations in both the line intensity and width are displayed. In both the spectra, the vibrational modes of the Tyr aromatic ring are well visible at around the 643 cm^{-1}, 830 cm^{-1}, 850 cm^{-1}, 1174 cm^{-1} and 1615 cm^{-1} frequencies, while the peaks associated to modes of Phe are located at 620 cm^{-1}, 1006 cm^{-1}, 1030 cm^{-1} and 1604 cm^{-1}. The peak around 950 cm^{-1} typically identifies the C–C stretching, while those at 750 cm^{-1} and 1341 cm^{-1} are related to the Trp vibrational modes. At about 1250 cm^{-1}, we observe the Amide III band as due to the in-phase combination of the N–H bending and the C–N stretching vibration and attributed to a mixture of secondary structures in protein solution.[44–46] The peak at about 1447 cm^{-1} arises from the CH_2–CH_3 deformation. Finally, the Amide I band, which is located within the 1620–1725 cm^{-1} spectral region, is mainly due to the C = O stretching vibration with minor contributions from the

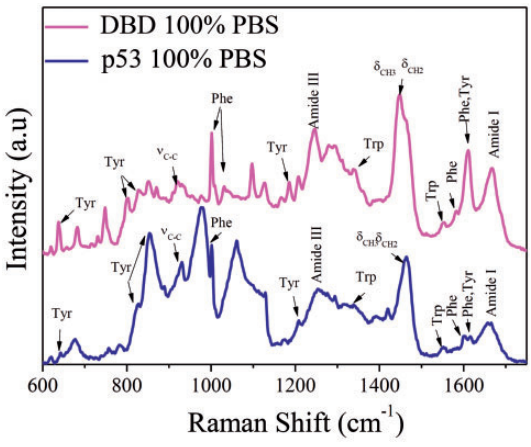

Figure 1. Raman spectra (600–1725 cm^{-1}) of DBD (magenta) and p53 (dark blue) in PBS at a concentration of 60 μM. Principal vibrational modes, Amide III and Amide I bands are marked (excitation at 532 nm).

out-of-phase C–N stretching vibration, the C–C–N deformation and the N–H in-plane bend.

We have focused our attention on the Amide I Raman band, which is well known to be strongly affected by the secondary structure architecture of the proteins.[36] Indeed, the excitonic coupling of Amide I modes comes from the vibrational coupling between motions of the peptide carbonyl groups organized in an ordered secondary structure through hydrogen bonds. An analysis of this band can provide detailed information on the structural conformation of the proteins in physiological conditions. We note that the Amide I band full width half-maximum (FWHM) of p53 ($50\,cm^{-1}$) is broader than that of DBD ($36\,cm^{-1}$). To closely investigate the secondary structural elements of both p53 and DBD, we have performed a careful deconvolution of the Amide I band by taking into account a method that is reported by Maiti et al.[36] In particular, the Amide I band has been fitted by considering a curve centered at 1650–$1656\,cm^{-1}$ and assigned to an α-helix, a second one at the 1664–$1670\,cm^{-1}$ region and attributed to β-sheet and a third one at about $1680\,cm^{-1}$, corresponding to random coil configurations. The integrated curve intensities fitting the Amide I band have been correlated with the contribution from the corresponding secondary structures under the assumption that the Raman cross-section is the same for each conformation. Indeed, we have found that the ratio of the Amide I band integrated area with that of the Tyr band, which is independent of secondary structure, did not exceed the 20% of variation in all conditions; this supports hypothesis according to Sane et al.[47]

The fitting curves of the Amide I Raman bands of DBD and p53 are shown in Figure 2, while the corresponding fitting parameters are reported in Table 1.

We remark that for DBD (Figure 2a) the β-component band centered at $1669\,cm^{-1}$ accounts for about 50% of the total integrated area and presents a BWHH of about $18\,cm^{-1}$. The α-helical band peak at $1655\,cm^{-1}$ contributes about 27% to the total Amide I band intensity with a BWHH of $20\,cm^{-1}$, while the random coil band at $1687\,cm^{-1}$ gives a 23% contribution to a BWHH with about $19\,cm^{-1}$. The propensity of DBD molecules to adopt a predominant β-sheet structure, with a lower random coil content, finds a correspondence with a large presence in the DBD sequence of hydrophobic residues (cysteine (Cys), Trp and leucine (Leu))[1,48] and it is in agreement with the crystallographic data.[18]

Concerning p53, we have revealed the presence of 50% of random coil conformations with lower percentages of α-helix and β-sheet structures (23% and 27%, respectively). It is important to remark that the corresponding fitting curves show higher BWHH values than in DBD; for example, the random coil band at $\sim 1675\,cm^{-1}$ (Figure 2b) being twice that in DBD (see Table 1). Such a behavior finds a correspondence with the large number of asparagine (Asp), lysine (Lys), arginine (Arg) and proline (Pro) residues that favor the formation of extended and flexible random coil regions.[48]

To further investigate the conformation populations of DBD and p53, we have adopted the strategy of modifying the solvent composition. In particular, we have taken into consideration mixtures of PBS with methanol (PBS/MeOH) or with 2,2,2-trifluoroethanol (PBS/TFE). Methanol is a polar alcohol, which is well known to strengthen the interactions between the polar backbone of the proteins and to enhance the formation of β-structures.[36,49,50] On the other hand, the hydrophobic nature of TFE permits interaction with the hydrophobic side chains in unfolded peptides and proteins, significantly affecting their solvation shell, stabilizing the α-helix structures through a combination of different physico–chemical effects (dielectric, coating, water stripping and thermodynamics effects).[51–53]

Figures 3 and 4 show the Raman spectra of DBD and p53 in PBS, PBS/MeOH and PBS/TFE, respectively. With a

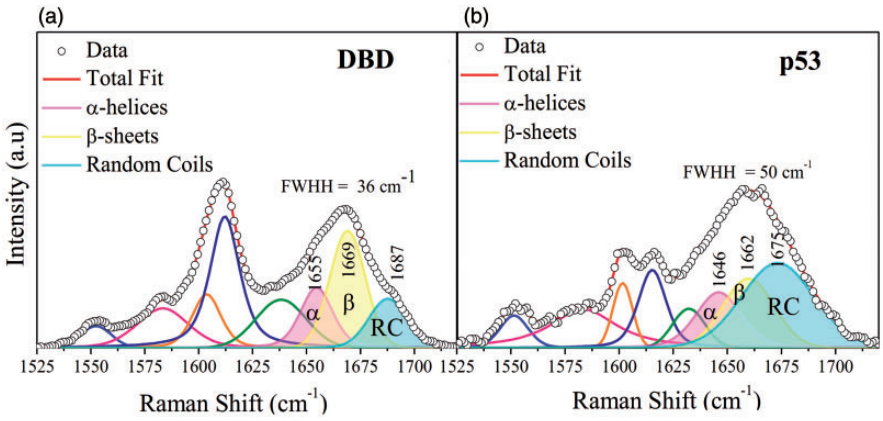

Figure 2. Experimental Amide I Raman spectra (open circles) of (a) DBD and (b) p53 in PBS, fitted using a three-component Voigt model (red line in each panel). The three bands associated to the main structural conformations of the protein are colored (magenta, α-helix; yellow, β-sheet; cyan, random coil).

Table 1. Results from the fitting procedure of the Amide I band of the DBD and p53 in PBS, PBS/MeOH and PBS/TFE. For each component (α-helix, β-sheet or random coil) the central frequency (cm^{-1}), the area (%) and the bandwidth (cm^{-1}) are reported. Area standard deviations are about ±10%, $\chi^2 = 0.002$, for all curve-fitting analysis.

Sample	DBD			p53			
	Secondary structure			Secondary structure			
Solvent	α-helix	β-sheet	RC	α-helix	β-sheet	RC	
PBS	1655	1669	1687	1646	1662	1675	Frequency (cm^{-1})
	27	50	23	23	27	50	Area (%)
	18	19	20	25	28	39	BWHH (cm^{-1})
PBS/MeOH	1654	1670	1688	1652	1667	1682	Frequency (cm^{-1})
	20	63	17	28	46	26	Area (%)
	19	22	22	17	18	25	BWHH (cm^{-1})
PBS/TFE	1655	1672	1687	1653	1669	1687	Frequency (cm^{-1})
	51	31	18	46	36	18	Area (%)
	25	19	20	20	24	23	BWHH (cm^{-1})

BWHH: bandwidth at half height; DBD: DNA binding domain; PBS: phosphate buffer solution; MeOH: methanol; TFE: Trifluoroethanol.

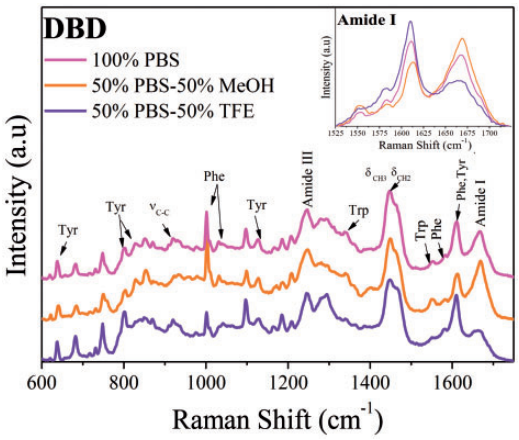

Figure 3. Raman spectra (600–1725 cm^{-1}) of DBD in PBS (magenta), in PBS/MeOH (orange) and PBS/TFE (violet), at a concentration of 60 μM. Inset: overlay of the Amide I bands in the three solvents. Principal vibrational modes, Amide III and Amide I bands of DBD are marked (Excitation at 532 nm).

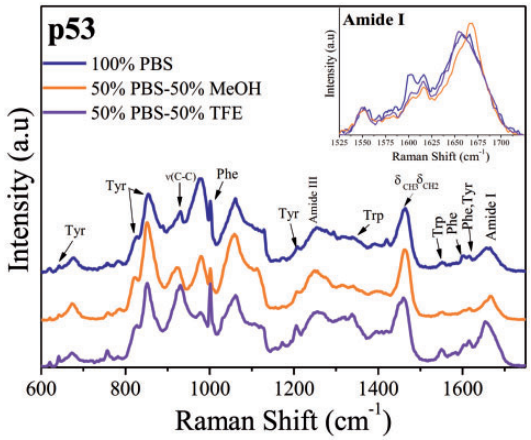

Figure 4. Raman spectra (600–1725 cm^{-1}) of p53 in PBS (dark blue), in PBS/MeOH (orange) and PBS/TFE (violet), at a concentration of 60 μM. Inset: overlay of the Amide I bands in the three solvents. Principal vibrational modes, Amide III and Amide I bands of p53 are marked (excitation at 532 nm).

visual inspection, no drastic changes in the spectral vibrational modes at low frequencies are induced by changing the solvents in both proteins. On the other hand, the FWHH of Amide I band of DBD undergoes a significant broadening (from ~36 cm^{-1} in PBS to ~50 cm^{-1} in TFE), while no variation is observed after the addition of MeOH. Furthermore, the Amide I width moves from ~50 cm^{-1} in PBS to ~35 cm^{-1} and ~47 cm^{-1}, in PBS/MeOH and PBS/TFE, respectively, in the p53 sample. To investigate such solvent-induced effects, again the Amide I bands have been analyzed.[36] The Amide I bands and all the fitting curves of DBD and p53 in PBS/MeOH and PBS/TFE solvents are shown in Figure 5; the corresponding fitting parameters are reported in Table 1.

We found that the β-sheet structures predominate in DBD in PBS/MeOH (Figure 5a), accounting for over 63% of the entire Amide I, while both the α-helix and random coil populations are reduced. At variance, in the PBS/TFE solution, the contribution of α-helix conformations drastically increases up to 51%, while the β-sheet amount significantly decreases to 31% and the random coil contribution remains almost the same (Figure 5b).

In p53, the addition of methanol induces an increase of β-sheet components up to 46%, while the random coil decreases from 50% (in PBS) to 26%. Finally, for p53 in PBS/TFE (Figure 5d), we note an increment of both the α-helical (46%) and the β-sheet structures (36%).

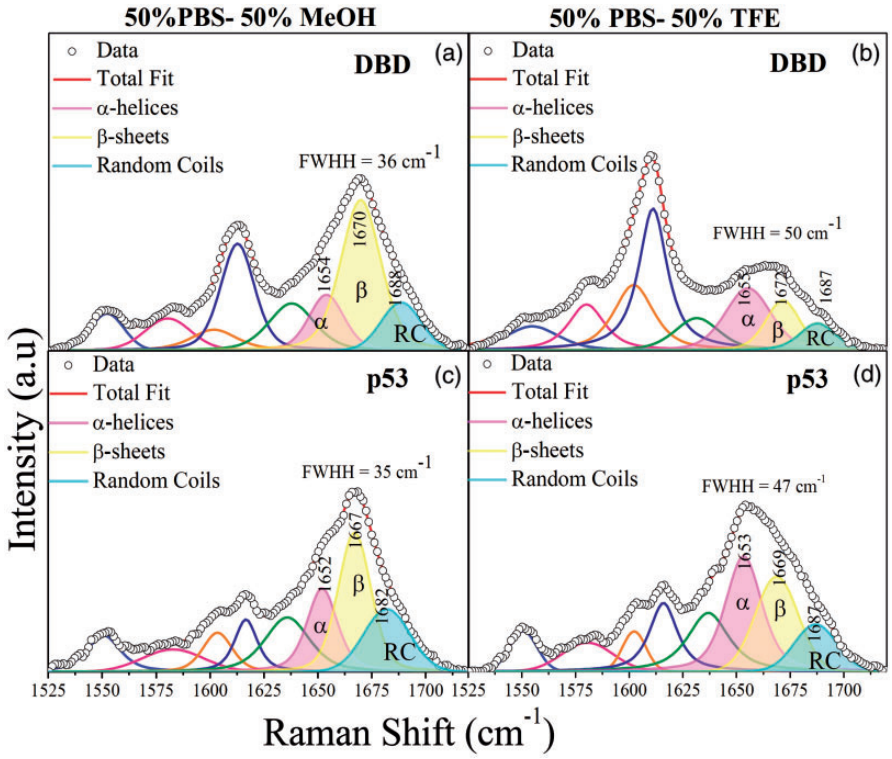

Figure 5. Experimental Amide I Raman spectra (open circles) of (a, b) DBD and (c, d) p53 in PBS/MeOH and in PBS/TFE, fitted using a three-component Voigt model (red line in each panels). (a) FWHH = 36 cm^{-1}; (b) FWHH = 50 cm^{-1}; (c) FWHH = 35 cm^{-1}; (d) FWHH = 47 cm^{-1}. The three bands associated to the main structural conformations of the protein are colored (magenta, α-helix; yellow, β-sheet; cyan, random coil).

Additionally, the random coil contribution strongly decreases down to 18% (see Table 1).

Concomitantly, with the variation of the structural distributions due to solvent perturbation, a significant narrowing of all the fitting curves' bandwidth has been observed (see Table 1). The simultaneous occurrence of the above mentioned effects upon varying the solvent composition, has been observed in Raman investigations of other IDPs, such as α-synuclein, β casein and phosvitin, and it has been associated to a decrease of the proteins' conformational disorder.[36] Indeed, the disorder character of IDPs derives from the presence of an ensemble of dynamically interchanging secondary conformations. On such a basis, under the assumption that the Amide I Raman band arises from a superposition of signals from different molecules adopting different conformations, the overall band narrowing could be indicative of a reduction in the structural distributions and then of a decrease of the protein conformational heterogeneity.[36]

The remarkable narrowing of the p53 Amide I bands observed on passing from PBS to PBS/MeOH and PBS/TFE thus suggests that a transition from a disordered conformational state to a more ordered one occurs. On the other hand, although DBD shows the same tendency of p53 to adopt different structural conformations by varying the solvents' composition, the less marked solvent-induced narrowing of its Amide I bands is indicative of a lower level of heterogeneity; this being consistent with the lower presence of unstructured regions in DBD and in agreement with crystallographic data.[16,17]

Principal Components Analysis of the Amide I Region

Figure 6a shows the PCA scores of PC1 vs PC2 components for the Amide I band of DBD and p53 in PBS, with these two components providing 67% of the total variance. In the scatter plot, two distinct groupings along the PC1 axis can be identified (see the ellipses drawn as a guide). Indeed, the DBD scores are located in the positive portion of the plot along PC1 with a large spread along both of the axes, while the p53 scores (filled symbols) display negative PC1 values, with a large variability along PC2. With the aim of correlating the position of the scores in the plot with the samples spectral features, we have analyzed the loadings with the variables mostly contributing to the PCA scores. As shown in Figure 6b, high levels of variance are detected in correspondence with the peaks at 1604 cm^{-1} and 1617 cm^{-1} related to Phe and Tyr modes, respectively. Weaker peaks are observed at 1550 cm^{-1}, corresponding to the Trp vibrational mode and at 1583 cm^{-1} related to a Phe mode.[36] Additionally, a high spectral variance is revealed in the 1630–1700 cm^{-1} range, where a broad

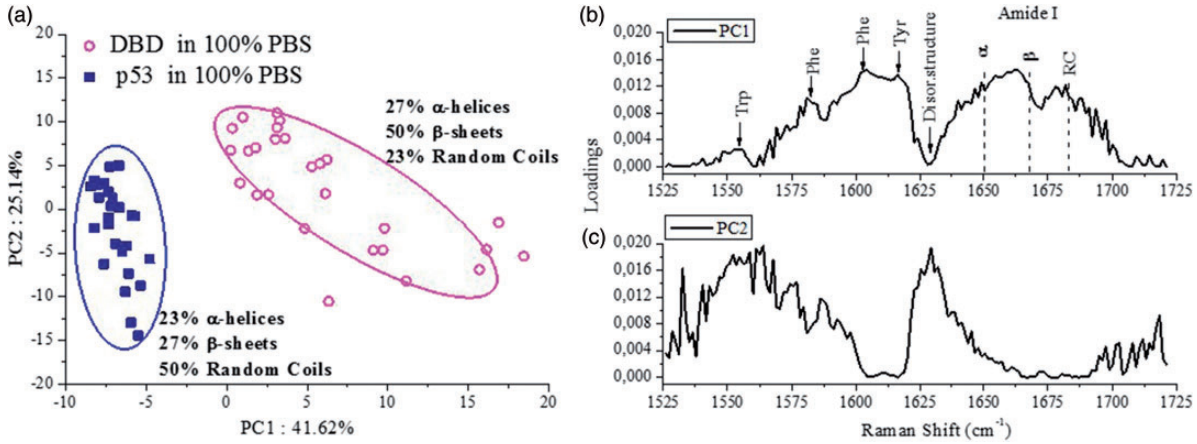

Figure 6. (a) Two-dimensional scores plot PC1 versus PC2 of the Raman spectra for DBD (magenta empty symbols) and p53 (blue filled symbols) in the PBS performed on the Amide I band. The two groupings are indicated by ellipses. The secondary structure percentages are also reported. (b) PC1 (42% of total variance) and (c) PC2 (25% of total variance) one-dimensional loadings plot versus frequency. The Raman markers are indicated.

band consistently appears with the presence of the α-helix (at about 1654 cm^{-1}), β-sheet (at 1668 cm^{-1}) and random coil (at 1680 cm^{-1}) structural components, as previously observed. The PC2 loading plot, providing complementary information to PC1, shows the largest variances in the 1525–1600 cm^{-1} region, which is related to the Trp mode, and in the 1630 cm^{-1} band, possibly associated to disordered regions[43] (see Figure 6(b)).

The evidence that the spectral differences between DBD and p53 are principally due to the Phe and Tyr vibrational modes finds a correspondence with other studies demonstrating the important role in p53 stability and biological activity of Tyr236[54] and Tyr327,[55] respectively. Meanwhile, a significant contribution to the total variance comes from the spectral region at 1630–1725 cm^{-1}.

Therefore, the PCA analysis, which is able to separate the Raman spectral features of proteins according to their structural differences, provides a confirmation of the results from the curve-fitting analysis.

We then applied PCA analysis to the Amide I Raman band of DBD and p53 in the three solvents. Two-dimensional plots have been constructed with different combinations of scores for the first three principal components (PC1, PC2 and PC3); only the components with the highest contribution to structural variables being shown.

Figure 7a shows the scatter plot of PC1 versus PC3 in the frequency range where the Amide I band is located for DBD in the three solvents (PBS, PBS/MeOH and PBS/TFE). Both DBD data in PBS (magenta circles) and in PBS/MeOH (orange stars) are characterized by negative values with a similar variability along both of the axes. DNA binding domain data in PBS/TFE (violet triangles) are at the upper-left corner of the plot, with a slightly lower variance with respect to other solvents. To find the most important contributions to the spectra, we investigated the PC1 loading, accounting for 39% of the variance. The highest values of variance are associated to a peak at 1637 cm^{-1}, possibly related to disordered structures,[43] and to a large band including the Trp and Phe modes (1550–1603 cm^{-1}). Additionally, we note a weaker peak at 1650 cm^{-1}, consistent with the α-helical component. In PC3, the major source of variance comes from the band at 1700 cm^{-1} with a lower contribution from the peak at 1650 cm^{-1}. Therefore, the separation among groups along PC3 occurs according to the secondary structure of the samples. On the other hand, the slight decrease of the spread passing from PBS to PBS/MeOH and to PBS/TFE reflects a similar structural distribution within each group, with a concomitant decrease of structural disorder.

Figure 8a shows the scatter plot of PC2 vs PC3 scores of p53 in PBS, PBS/MeOH and PBS/TFE. Notably, the data are clustered into three distinct groups along the PC2 axis (see the ellipses drawn as a guide). In particular, p53 in PBS (blue squares) is mainly grouped in the upper side of the scatter plot with a rather large spread along both the PC2 and PC3 directions. The p53 protein in PBS/MeOH (orange stars) falls in the lower-right part of the plot, presenting a slightly lower spread than that in PBS. Moreover, p53 in PBS/TFE (violet triangles) is located at the lower-left corner of the plot and is characterized by negative values along both the axes. Again, the loading plots have been examined in order to identify the variable responsible for discrimination among the p53 classes. In Figure 8b PC2 presents high values at 1550 cm^{-1}, 1603 cm^{-1} and 1615 cm^{-1}, corresponding to the Trp, Phe and Tyr vibrational frequencies, respectively, while a lower contribution is from a peak at 1637 cm^{-1}. Interestingly, the highest variance occurs at the ~1650 cm^{-1} and ~1668 cm^{-1} frequencies, which are ascribed to the α-helix and β-sheet constituents of the Amide I band, with a minor source of positive variance

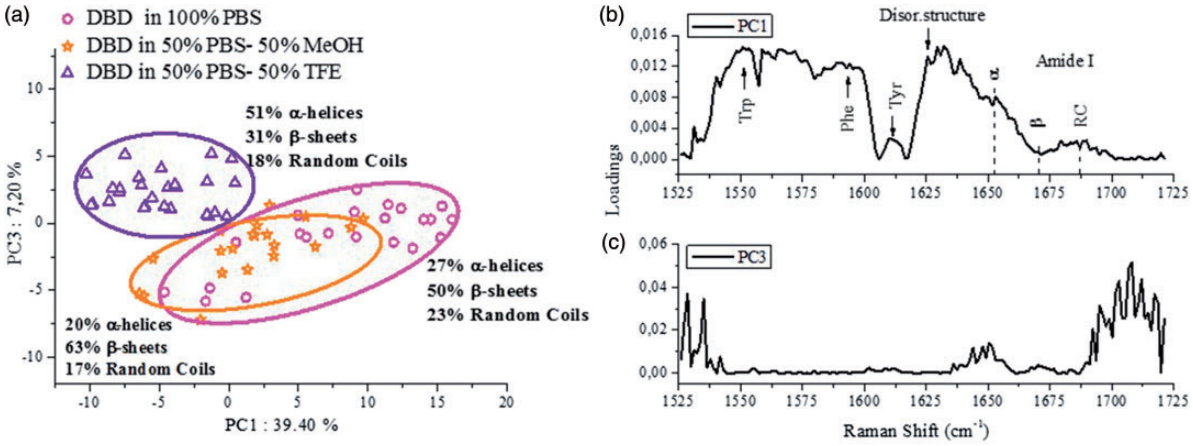

Figure 7. (a) Two-dimensional scores plot PC1 versus PC3 of the Raman spectra for DBD in the PBS (magenta symbols), PBS/MeOH (orange symbols) and PBS/TFE (violet symbols) solvents performed on the Amide I band. The three groupings are indicated by ellipses. The secondary structure percentages are also reported. (b) PC1 (39% of total variance) and (c) PC3 (7% of total variance) one-dimensional loadings plot versus frequency. The Raman markers are indicated.

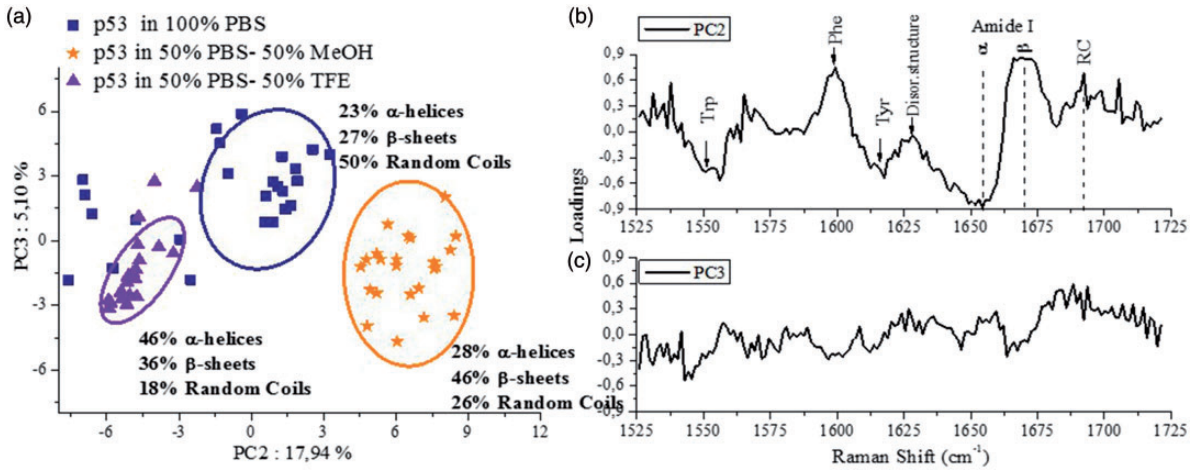

Figure 8. (a) Two-dimensional scores plot PC2 versus PC3 of the Raman spectra for p53 in the PBS (dark blue symbols), PBS/MeOH (orange symbols) and PBS/TFE (violet symbols) solvents performed on the Amide I band. The three groupings are categorized by ellipses drawn as a guide. The secondary structure percentages are also reported. (b) PC2 (18% of total variance) and (c) PC3 (5% of total variance) one-dimensional loadings plot versus frequency. The Raman markers are indicated.

coming from the $\sim$1680 cm^{-1} frequency. This indicates a negative correlation between the amount of α-helix and both the β-sheet and random coil conformations. In the PC3 loadings plot (Figure 8b), accounting for 5% of the variation in the spectra, the highest source of spectral variance is associated to the 1680 cm^{-1} band. A loading curve inspection for PC2 shows that the discrimination among the p53 samples reflects the amount of α-helix and β-sheet conformations. Indeed, we note that the α-helix β-sheet ratio within each group, (see the curve-fitting values in Figure 8a), progressively decreases, moving from the negative left side of the plot toward the right side. In addition, the amount of the ordered structure (i.e., α-helix + β-sheet) increases, passing from the upper level of the plot to the lower level. Furthermore, the p53 scores in PBS/TFE (Figure 8a), are very close to each other, indicating a lower variability than in other solvents. On the basis of the loadings results, such an effect suggests a decrease of the protein disorder as induced by the PBS/TFE solvent. This effect is in agreement with previous results that show a drastic reduction of random coil conformations as induced by PBS/TFE solvent. Furthermore, the partial overlapping among different clusters finds a correspondence with the tendency of p53 to populate an ensemble of different conformations.

These results are evidence that PCA has a high capability for effectively discriminating between p53 and its DNA-binding domain on the basis of their structural differences. Moreover, it has also been found to be sensitive to changes

in the secondary structure content within the same sample, outlining changes in the conformational heterogeneity.

Conclusions

Raman spectroscopy has been demonstrated to be an effective tool for disclosing the main structural motifs of p53 IDPs and its DBD region. The deconvolution of the Amide I band, remarkably sensitive to the α-helix, β-sheets and random coil structures, has allowed us to assess the main structural motifs of these proteins. In particular, a careful fitting procedure of this band has revealed that about 50% of native full-length p53 displays a random coil structure, while the rest is almost equally shared between α-helix and β-sheets structures. Conversely, β-sheets (50%) are the prevailing structure of DBD, with the remaining regions being uniformly distributed between α-helix and random coil structures. An analysis of p53 in different solvents has shown a reduction of protein conformational heterogeneity, as revealed by a solvent-induced decrease of the conformational distributions. On the other hand, the detection of a weaker solvent-induced effect in DBD pointed out its prevailing native ordered structure. The solvent perturbations of the DBD and p53 conformational distribution might involve the coexistence of different factors, such as thermodynamic processes, presumably via enthalpic and entropic effects, or water-stripping phenomena related to solvent polarity dielectric effects. Furthermore, PCA applied to the Amide I band has been successful in identifying the most significant spectral features of DBD and p53 by also revealing the Raman spectral characteristics in the different solvent environments. These combined approaches have displayed a high capability for unraveling the structure and conformational heterogeneity of IDPs. Accordingly, such a strategy could be helpful in improving the structural characterization of other biologically important proteins. In particular, this could be extended to disclosing the structural motifs of mutated forms of p53, which, having a crucial role in human cancer, may represent the preferential target for novel therapeutic applications.

Conflict of Interest

None declared.

Funding

This work was supported by the Italian Association for Cancer Research (grant number AIRC No 15866) and by a PRIN-MIUR 2012 Project (grant number 2012NRRP5J).

References

1. V.N. Uversky. "Unusual Biophysics of Intrinsically Disordered Proteins". Biochim Biophys Acta. 2013. 1834(5): 932–951.
2. J.D. Forman-Kay, T. Mittag. "From Sequence and Forces to Structure, Function, and Evolution of Intrinsically Disordered Proteins". Structure. 2013. 21(9): 1492–1498.
3. M.M. Babu, R. Van Der Lee, N. Sanchez De Groot, J. Gsponer. "Intrinsically Disordered Proteins: Regulation and Disease". Curr. Opin. Struct. Biol. 2011. 21(3): 432–440.
4. P.E. Wright, H.Y. Dyson. "Intrinsically Unstructured Proteins: Re-assessing the Protein Structure-Function Paradigm". J. Mol. Biol. 1999. 293(2): 321–331.
5. J.J. Ward, J.S. Sodhi, L.J. Mcguffin, B.F. Buxton, D.T. Jones. "Prediction and Functional Analysis of Native Disorder in Proteins from the Three Kingdoms of Life". J. Mol. Biol. 2004. 337(3): 635–645.
6. A. Lobley, M.B. Swindells, C.A. Orengo, D.T. Jones. "Inferring Function Using Patterns of Native Disorder in Proteins". PLoS Comput. Biol. 2007. 3(8): E162.
7. L.M. Iakoucheva, C.J. Brown, J.D. Lawson, Z. Obradovic, A.K. Dunker. "Intrinsic Disorder in Cell-Signaling and Cancer-Associated Proteins". J Mol. Biol. 2002. 323(3): 573–584.
8. V.N. Uversky, C.J Oldfield, A.K Dunker. "Intrinsically Disordered Proteins in Human Diseases Introducing the D2 Concept". Annu. Rev. Biophys. 2008. 37: 215–246.
9. H. Hegyi, L. Buday, P. Tompa. "Intrinsic Structural Disorder Confers Cellular Viability on Oncogenic Fusion Proteins". Plos Comput. Biol. 2009. 5(10): E1000552.
10. C.J. Oldfield, J. Meng, J.Y. Yang, M.Q. Yang, V.N. Uversky, A.K. Dunker. "Flexible Nets: Disorder and Induced Fit in the Associations of p53 and 14-3-3 with their Partners". BMC Genomics. 2008. 9(Suppl 1): S1.
11. C. Andresen, S. Helander, A. Lemak, C. Fares, V. Csizmok, J. Carlsson, L.Z. Penn, J.D. Forman-Kay, C.H. Arrowsmith, P. Lundström, M. Sunnerhagen. "Transient Structure and Dynamics in the Disordered c-Myc Transactivation Domain Affect Bin1 Binding". Nucleic Acids Res. 2012. 40(13): 6353–6366.
12. B. Vogelstein, S. Sur, C. Prives. "P53: The Most Frequently Altered Gene in Human Cancers". Nature Education. 2010. 3(9): 6.
13. R. Dawson, L. Muller, A. Dehner, C. Klein, H. Kessler, J. Buchner. "The N-Terminal Domain of p53 is Natively Unfolded". J. Mol. Biol. 2003. 332(5): 1131–1141.
14. P. Tompa. "Intrinsically Disordered Proteins: A 10-Year Recap". Trends in Biochem. Sci. 2012. 37(12): 509–516.
15. S. Bell, C. Klein, L. Muller, S. Hansen, J. Buchner. "P53 Contains Large Unstructured Regions in its Native State". J. Mol. Biol. 2002. 322(5): 917–927.
16. J.M.P. Cañadillas, H. Tidow, S.M.V. Freund, T.J. Rutherford, H.C. Ang, A.R. Fersht. "Solution Structure of p53 Core Domain: Structural Basis for its Instability". Proc. Natl. Acad. Sci. USA. 2006. 103(7): 2109–2114.
17. Y. Cho, S. Gorina, P.D. Jeffrey, N.P. Pavletich. "Crystal Structure of a p53 Tumor Suppressor-DNA Complex: Understanding Tumorigenic Mutations". Science. 1994. 265(5170): 346–355.
18. A.C. Joerger, A.R. Fersht. "The Tumor Suppressor P53: From Structures to Drug Discovery". Cold Spring Harb. Perspect. Biol. 2010. 2(6): A000919.
19. L. Collavin, A. Lunardi, G. Del Sal. "P53-Family Proteins and their Regulators: Hubs and Spokes in Tumor Suppression". Cell Death Differ. 2010. 17(16): 901–911.
20. A.R. Bizzarri, S. Santini, E. Coppari, M. Bucciantini, S. Di Agostino, T. Yamada, C.W. Beattie, S. Cannistraro. "Interaction of an Anticancer Peptide Fragment of Azurin with p53 and its Isolated Domains Studied by Atomic Force Spectroscopy". Int. J. Nanomed. 2011. 6: 3011−3019.
21. A.R. Bizzarri, S. Di Agostino, L. Andolfi, S. Cannistraro. "A Combined Atomic Force Microscopy Imaging and Docking Study to Investigate the Complex Between p53 DNA Binding Domain and Azurin". J. Mol. Recognit. 2009. 22(6): 506–515.
22. V. De Grandis, A.R. Bizzarri, S. Cannistraro. "Docking Study and Free Energy Simulation of the Complex Between p53 DNA-Binding Domain and Azurin". J. Mol. Recognit. 2006. 20(4): 215–226.
23. F. Domenici, A.R. Bizzarri, S. Cannistraro. "SERS-Based Nanobiosensing for Ultrasensitive Detection of the p53 Tumor Suppressor". Int. J. Nanomed. 2011. 6: 2033–2042.

24. F. Domenici, A.R. Bizzarri, S. Cannistraro. "Surface-Enhanced Raman Scattering Detection of Wild-Type and Mutant p53 Proteins at Very Low Concentration in Human Serum". Anal. Biochem. 2012. 421(1): 9–15.
25. M. Taranta, A.R. Bizzarri, S. Cannistraro. "Modeling the Interaction Between the N-Terminal Domain of the Tumor Suppressor p53 and Azurin". J. Mol. Recognit. 2009. 22(3): 215–222.
26. A.N. Bullock, J. Henckel, B.S. Dedecker, C.M. Johnson, P.V Nikolova, M.R. Proctor, D.P. Lane, A.R. Fersht. "Thermodynamic Stability of Wild-Type and Mutant p53 Core Domain". Proc. Natl. Acad. Sci. USA. 1997. 94(26): 14338–14342.
27. S. Lukman, D.P. Lane, C.S. Verma. "Mapping the Structural and Dynamical Features of Multiple p53 DNA Binding Domains: Insights into Loop 1 Intrinsic Dynamics". PLoS ONE. 2013. 8(11): 1–17.
28. A.C. Joerger, H.C. Ang, D.B. Veprintsev, C.M. Blair, A.R. Fersht. "Structures of p53 Cancer Mutants and Mechanism of Rescue by Second-Site Suppressor Mutations". J. Biol. Chem. 2005. 280(16): 16030–16037.
29. H. Viadiu. "Molecular Architecture of Tumor Suppressor P53". Curr. Top Med. Chem. 2008. 8(15): 1327–1334.
30. P.E. Wright, H.J. Dyson. "Intrinsically Disordered Proteins in Cellular Signaling and Regulation". Nat. Rev. Mol. Cell Biol. 2015. 16(1): 18–29.
31. C.K. Fisher, C.M. Stultz. "Constructing Ensembles for Intrinsically Disordered Proteins". Curr. Opin. Struct. Biol. 2011. 21(3): 426–431.
32. P. Bernadó, D.I. Svergun. "Structural Analysis of Intrinsically Disordered Proteins by Small-Angle X-ray Scattering". Mol. Biosyst. 2012. 8(1): 151–167.
33. J.A. Marsh, J.D. Forman-Kay. "Ensemble Modeling of Protein Disordered States: Experimental Restraint Contributions and Validation". Proteins. 2011. 80(2): 556–572.
34. R. Schneider, J.R. Huang, M. Yao, G. Communie, V. Ozenne, L. Mollica, L. Salmon, M.R. Jensen, M. Blackledge. "Towards a Robust Description of Intrinsic Protein Disorder Using Nuclear Magnetic Resonance Spectroscopy". Mol. Biosyst. 2012. 8(1): 58–68.
35. R. Tuma. "Raman Spectroscopy of Proteins: From Peptides to Large Assemblies". J. Raman Spectrosc. 2005. 36(4): 307–319.
36. N.C. Maiti, M.M. Apetri, M.G. Zagorski, P.R. Carey, V.E. Anderson. "Raman Spectroscopic Characterization of Secondary Structure in Natively Unfolded Proteins: α-Synuclein". J. Am. Chem. Soc. 2004. 126(8): 2399–2408.
37. T. Yamada, S. Signorelli, S. Cannistraro, C.W. Beattie, A.R. Bizzarri. "Chirality Switching Within a Cell-Penetrating Peptide Inhibits Translocation Without Affecting Preferential Entry". Mol. Pharm. 2014. 12(1): 140–149.
38. M. Ringnér. "What is Principal Component Analysis?". Nat. Biotechnol. 2008. 26(3): 303–304.
39. N. Alizadeh-Pasdar, S. Nakai, E.C.Y. Li-Chan. "Principal Component Similarity Analysis of Raman Spectra to Study the Effects of Ph, Heating, and K-Carrageenan On Whey Protein Structure". J. Agric. Food Chem. 2002. 50(21): 6042–6052.
40. S. Pieters, Y.V. Heyden, J.-M. Roger, M. D'Hondt, L. Hansen, B. Palagos, B. De Spiegeleer, J.-P. Remon, C. Vervaet, T. De Beer. "Raman Spectroscopy and Multivariate Analysis for the Rapid Discrimination Between Native-Like and Non-Native States in Freeze-Dried Protein Formulations". Eur. J. Pharm. Biopharm. 2013. 85(2): 263–271.
41. J. Ye, S.A. Fox, M. Cudic, E.M. Rezler, J.L. Lauer, G.B. Fields, A.C. Terentis. "Determination of Penetratin Secondary Structure in Live Cells with Raman Microscopy". J. Am. Chem. Soc. 2010. 132(3): 980–988.
42. V.J.C. Lin, J.L. Koenig. "Raman Studies of Bovine Serum Albumin". Biopolymers. 1976. 15(1): 203–218.
43. K. Huang, N.C. Maiti, N.B. Phillips, P.R. Carey, M.A. Weiss. "Structure-Specific Effects of Protein Topology On Cross-β Assembly: Studies of Insulin Fibrillation". Biochem. 2006. 45(34): 10278–10293.
44. T. Miura, T. Miura. "Raman Spectroscopy of Proteins and their Assemblies". In: G.J Biswas, S. Thomas Jr (eds) Subcellular Biochemistry: Proteins: Structure, Function, and Engineering. New York: Plenum Press, 1995, pp.55–99.
45. L. Laporte, J. Stultz, G.J. Thomas Jr. "Solution Conformations and Interactions of α and β Subunits of the Oxytricha Nova Telomere Binding Protein: Investigation by Raman Spectroscopy". Biochem. 1997. 36(26): 8053–8059.
46. S. Krimm, J. Bandekar. "Vibrational Spectroscopy and Conformation of Peptides, Polypeptides, and Proteins". J. Adv. Protein Chem. 1986. 38: 181–364.
47. S.U. Sane, S.M. Cramer, T.M. Przybycien. "A Holistic Approach to Protein Secondary Structure Characterization Using Amide I Band Raman Spectroscopy". Anal. Biochem. 1999. 269(2): 255–272.
48. V.N. Uversky, C.J. Oldfield, U. Midic, H Xie, B. Xue, S. Vucetic, L.M. Iakoucheva, Z. Obradovic, A.K. Dunker. "Unfoldomics of Human Diseases: Linking Protein Intrinsic Disorder with Diseases". BMC Genomics. 2009. 10(Suppl. 1): S7.
49. M. Fioroni, M.D. Diaz, K. Burger, S. Berger. "Solvation Phenomena of a Tetrapeptide in Water/Trifluoroethanol and Water/Ethanol Mixtures: A Diffusion NMR, Intermolecular NOE, and Molecular Dynamics Study". J. Am. Chem. Soc. 2002. 124(26): 7737–7744.
50. L.A. Munishkina, C. Phelan, V.N. Uversky, A.L. Fink. "Conformational Behavior and Aggregation of Alpha-Synuclein in Organic Solvents: Modeling the Effects of Membranes". Biochem. 2003. 42(9): 2720–2730.
51. S. Fatima, B. Ahmad, R. Hasan Khan. "Fluoroalcohols Induced Unfolding of Succinylated Con A: Native Like β-Structure in Partially Folded Intermediate and α-Helix in Molten Globule Like State". Arch. Biochem. Biophys. 2006. 454(2): 170–180.
52. K. Gast, D. Zirwer, M. Muller-Frohne, G. Damaschun. "Trifluoroethanol-Induced Conformational Transitions of Proteins: Insights Gained from the Differences Between α-Lactalbumin and Ribonuclease A". Protein Sci. 1999. 8(3): 625–634.
53. P. Gupta, R.H. Khan, M. Saleemuddin. "Trifluoroethanol-Induced "Molten Globule" State in Stem Bromelain". Arch. Biochem. Biophys. 2003. 413(2): 199–206.
54. A. Madhumalar, D. John Smith, C. Verma. "Stability of the Core Domain of P53: Insights from Computer Simulations". BMC Bioinformatics. 2008. 9(Suppl 1): S17.
55. V.A. Yakovlev, A.S. Bayden, P.R. Graves, G.E. Kellogg, R.B. Mikkelsen. "Nitration of the Tumor Suppressor Protein p53 at Tyrosine 327 Promotes p53 Oligomerization and Activation". Biochem. 2010. 49(25): 5331–5339.